Multilayered shell model with variable representation of displacements across the thickness

Multilayered shell model with variable representation of displacements across the thickness

U. Icardi*, L. Ferrero [1]

Dipartimento di Ingegneria Aeronautica e Spaziale, Politecnico di Torino, Corso Duca degli Abruzzi 24, 10129 Torino, Italy

ABSTRACT
A multilayered zig-zag shell model is developed; it has a hierarchic representation of displacements across the thickness that a priori fulfils the interfacial stress contact conditions on interlaminar shear and normal stresses. Like for classical models, the functional d.o.f. are the mid-plane displacements and the shear rotations. Characteristic feature, the representation can vary from point to point across the thickness, in order to adapt to the variation of solutions. The coefficients of the higher-order terms are determined as functions of the d.o.f. by enforcing equilibrium conditions at discrete points across the thickness. The Lame's coefficients are expanded up to the second order. As shown by the numerical tests, it accurately predicts the stress fields of thick laminated and sandwich shells with abruptly chang-ing material properties with a lower overall processing time

Keywords:
A. Layered structures
B. Elasticity
C. Analytical modelling
C. Computational modelling

1. Introduction

Owing to their advantageous properties, laminated and sandwich composites are finding an increasing number of applications in various engineering fields. Since they can absorb a large amount of energy by micro-structure failures, a serious design concern is their damage accumulation in service. In the regions where damage rises, the out-of-plane stresses and strains become as important as their in-plane counterparts for keeping equilibrium and satisfying the boundary conditions. Furthermore, sandwiches need an accurate modelling of the transverse normal stress and deformation, since the core can crush. A variety of models have been recently developed that provide a kinematically correct representation of the cross-sectional warping associated with the deformation of multilayered structures, i.e. the so-called "zig-zag" behaviour (see, e.g., Savoia and Reddy [1,2] and Savoia et al. [3]). These models, that are known as layerwise models – LWM, feature displacements continuous across the thickness but, in order to allow for continuous equilibrating interlaminar stresses, with discontinuous derivatives with respect to the thickness coordinate at the layer interfaces. A comprehensive review being beyond the purpose of the present paper, the readers are referred to the recent survey papers and books that discuss the distinctive features, merits and drawbacks in terms of solution accuracy and economy of LWM (see, among many others, Burton and Noor [4] and Reddy [5]). Aimed at accounting for the effects of damage with the ideal combinations of accuracy and efficiency required for developing safe, damage tolerant structures, the research on LWM is still fervent. To put the contribution of this paper in the right perspective, a broad discussion of the basic features of LWM is given, where only the most relevant concepts and few representative papers will be cited.

According with the current terminology, LWM are referred as full or partial models whether the transverse normal strain is considered or neglected. It is here reminded the importance of this strain and of the related stress for keeping equilibrium in the regions around holes, cutouts, free edges, delamination fronts and discontinuities in general, besides for core crushing of sandwiches.

LWM can also be classified into (i) models with a number of functional d.o.f. depending on the number of constituent layers, and (ii) models with a fixed number of functional d.o.f. The former class (i) comprises full or partial LWM in form of discrete-layer models – DL (see, e.g., Reddy [6]), exact solutions of simplified cases (see, e.g., Ren [7] and Wu et al. [8]) and full three-dimen-sional models (see, e.g., Sheng and Ye [9]), either in displacement based or mixed form (see, e.g., Wu and Liu [10]) and of 2-D or 3-D types.

The basic difference of DL models with respect to exact solutions lies on the assumptions made about the distribution of displacements and stresses across the thickness. In the widespread, versatile DL models, piecewise approximations are made across the thickness of each constituent layer, consequently accuracy, processing time and memory occupation grow with the number

* Corresponding author. Tel : +39 (0)11 5646872; fax: +39 (0)11 5646899.
E-mail addresses: ugo.icardi@polito.it (U. Icardi), laura.ferrero.ext@siemens.com (L. Ferrero).
[1] Present address: TurboCare SpA, Corso Romania 661, 1056 Torino, Italy.

of computational layers. For not overwhelming the computational capacity their use should be restricted to a detailed analysis in localised regions. Various techniques have been developed for making computationally efficient the enforcement of the contact conditions at the interfaces. As examples, the papers by Ascione and Fraternali [11] and Fraternaly and Reddy [12] are cited, in which the penalty method is used.

Models that can have partial of full 3-D modelling capability, as desired, have been developed as finite elements aimed at limiting the computational costs. Known as hierarchical multilayered FEM models, they assume different types of displacement fields in the same problem, namely an underlying foundation provided by and equivalent single layer model – ESL that constitutes the global part, and an optional incremental enhancement provided by a lay-erwise model that constitutes the local part (see, e.g., Barbero and Reddy [13]). Predictor–corrector iterational models have been developed with the same purpose, in which the information ob-tained in the predictor phase is used to correct key elements in the corrector phase. Usually an ESL model is used for computing initial estimates, while a DL model is used for corrections (see,
e.g., Lee and Cao [14]).

The above mentioned class (ii) of models with fixed d.o.f. comprises equivalent single-layer models (see, e.g., Dennis and Palazotto [15], and Jing and Tzeng [16]) that assume the multilayered structures as an equivalent single layer (consequently the number of functional d.o.f. is independent of the number of constituent layers) and zig-zag models – ZZ (see, e.g., Di Sciuva [17], Di Sciuva and Icardi [18], Xavier et al. [19], Cho et al. [20], Icardi [21], Icardi and Ruotolo [22], and Oh and Cho [23]) that *a priori* fulfil the displacement and stress contact conditions at the inter-faces of the constituent layers by incorporating continuity functions that are determined once for all for any lamination se-quence. They can be as accurate as DL models if post-processing procedures are employed, the properties are not abruptly chang-ing, the thickness is not extreme and anisotropy is not severe. Plate models that combine the concepts of ZZ and DL models have been recently developed by Averill and co-workers [24–28]. They group several layers into a computational layer, like the ZZ models, with the purpose of containing the computational effort and stack computational layers for improving accuracy, like the DL models. Since many computational layers should be stacked and/or post-processing procedures should be employed for accurately predicting the stresses of damaged sandwiches, their advantages can be only apparent as shown in Ref. [29]. Moreover, cases exist for which the stresses computed by post-processing methods can be still not accurate enough in comparison with three-dimensional elasticity solutions (see Cho et al. [30]).

An improved ZZ plate model based on a global–local superposition technique aimed at accurately predicting the stress fields of thick components grouping all the physical layers and without any post-processing has been recently developed by Li and Liu [31], while a multilayered shell model has been developed by Zhen and Wanji [32]. It could be noticed that most of the multilayered shell models available in the literature are extensions of counterpart plate models. As examples, the following papers by Reddy and Liu [33], Dennis and Palazotto [34], Xavier et al. [35], Jing and Tzeng [36], Reddy and Starnes [37], Savoia and Reddy [38], Cho et al. [39] and Fraternali and Bilotti [40] are cited, that represent the extension of layerwise plate models based on different ideas.

In the global–local models mentioned above, which have 17 functional d.o.f., the transverse displacement is still assumed constant across the thickness. Recently, Vidal and Polit [41] have developed a 6 d.o.f. ZZ beam model based on the global–local superposition technique, with a parabolic transverse displacement and a sinusoidal representation of the in-plane displacement across the thickness. The basic advantage of these global–local ZZ models is that the increase of storage dimension with respect to classical plate models with 5 d.o.f. is compensated by the reduction of the overall processing time, since post-processing is unnecessary. They appear advantageous over DL models, since they achieve the same accuracy with a lower computational effort, having less functional d.o.f.

The contribution of the present paper is to explore whether a shell model with the five classical middle surface functional d.o.f. (i.e., the three displacements and the two shear rotations) and a hierarchic zig-zag representation of displacements also makes post-processing unnecessary for obtaining accurate stress predictions. The idea of an adaptive model was pioneered by the authors in Ref. [42] considering a mixed plate model with the displacements and the interlaminar stresses at the upper and lower surfaces of the computational layers as functional d.o.f. Herein the idea is extended to a shell model with the mid-plane standard d.o.f. It features a high-order, piecewise representation of the three displacement compo-nents across the thickness, that *a priori* fulfils the interfacial stress contact conditions on interlaminar shear and normal stresses. To this purpose, "continuity" functions are enclosed, that are deter-mined once for all for any lay-up enforcing the contact conditions at the interfaces. The present model represents a shell extension of a former zig-zag plate model by the authors, but it also extends the idea of hierarchical multilayered finite elements, the hierarchi-cal representation being incorporated directly into the displace-ment model, instead in the shape functions.

2. The present shell model

2.1. Characteristic features

The present shell model with displacements of variable order that adapt to the variation of solutions is obtained incorporating into the shell model of Ref. [22] the ZZ displacement field model of Ref. [43], here referred as the "basic model", then incorporating terms with higher-order powers of the thickness coordinate. The functional d.o.f. are the three displacement components and the two shear rotations of the normals at the reference surface, since the coefficients of the higher-order terms are expressed as functions of the d.o.f. of the basic model and their derivatives by enforcing equilibrium conditions at discrete points across the thickness. Other characteristic feature, the model *a priori* fulfils the interlaminar shear and normal stress contact conditions at the interfaces of the constituent layers, as prescribed by the elasticity theory. Moreover, it can provide accurate stress predictions from constitutive equations. A higher-order representation of the transverse displacement is considered aimed at accounting for the core crushing mechanism of sandwich shells. In addition, the model also achieves an improved strain energy description that would be precluded to post-processing techniques, which should be relevant for investigating energy absorption/dissipation mechanisms and for optimisation [44,45].

With the present model, higher-order terms are used only when necessary, while the computation of the continuity constants and coefficients of higher-order powers is required just once for all. The numerical results show that the present through-the-thickness hierarchic representation of the d.o.f. is advantageous, since it achieves the same accuracy of current post-processing techniques requiring a lower computational effort.

2.2. Notations

The middle surface Ω is assumed as the shell reference surface and the curvilinear tri-orthogonal system constituted by the lines α, β of principal curvature and the coordinate across the thickness

ζ as the reference system. The position of the upper$^+$ and lower$^-$ surfaces of the generic layer k are indicated as $^{(k)}\zeta^+$ and $^{(k)}\zeta^-$; the quantities that belong to a generic layer k are denoted with the suffix$^{(k)}$; u_α, u_β, u_ζ represent the elastic displacements in the direction of α, β and ζ; $R_\alpha(\alpha,\beta)$ and $R_\beta(\alpha,\beta)$ are the radii. The differentiation with respect to the spatial ordinates is denoted by the symbols $()_{,\alpha}$, $()_{,\beta}$. The Lamé coefficients are indicated as $A_\alpha(\alpha,\beta)$, $A_\beta(\alpha,\beta)$ on Ω and as H_α^{-1} (α,β,ζ), $H_\beta^{-1}(\alpha,\beta,\zeta)$ at a distanceζ.

2.3. Strains

The elastic displacements being supposed small, the following linear strain–displacement relations are assumed, as in the previ-ous shell models [21,22] ($H_\zeta = 1$):

$$\varepsilon_{\alpha\alpha} = \frac{u_{\alpha,\alpha}}{H_\alpha} + \frac{H_{\alpha,\beta}}{H_\alpha H_\beta}u_\beta + \frac{H_{\alpha,\zeta}}{H_\alpha H_\zeta}u_\zeta \tag{1}$$

$$\varepsilon_{\beta\beta} = \frac{u_{\beta,\beta}}{H_\beta} + \frac{H_{\beta,\alpha}}{H_\alpha H_\beta}u_\alpha + \frac{H_{\beta,\zeta}}{H_\beta H_\zeta}u_\zeta \tag{2}$$

$$\varepsilon_{\alpha\beta} = \frac{H_\alpha}{H_\beta}\left(\frac{u_\alpha}{H_\alpha}\right)_{,\beta} + \frac{H_\beta}{H_\alpha}\left(\frac{u_\beta}{H_\beta}\right)_{,\alpha} \tag{3}$$

$$\varepsilon_{\alpha\zeta} = \frac{H_\alpha}{H_\zeta}\left(\frac{u_\alpha}{H_\alpha}\right)_{,\zeta} + \frac{H_\zeta}{H_\alpha}\left(\frac{u_\zeta}{H_\zeta}\right)_{,\alpha} \tag{4}$$

$$\varepsilon_{\beta\zeta} = \frac{H_\beta}{H_\zeta}\left(\frac{u_\beta}{H_\beta}\right)_{,\zeta} + \frac{H_\zeta}{H_\beta}\left(\frac{u_\zeta}{H_\zeta}\right)_{,\beta} \tag{5}$$

$$\varepsilon_{\zeta\zeta} = \frac{1}{H_\zeta}u_{\zeta,\zeta} \tag{6}$$

The transverse displacement u_ζ is assumed to vary across the thickness for describing the core crushing mechanism. As in Ref. [22], the reciprocals of the Lamé coefficients $1/H_\alpha$, $1/H_\beta$ are approximated up to a second-order expansion with respect to ζ/R_α, ζ/R_β:

$$\frac{1}{H_\alpha} = \frac{1}{A_\alpha}\left(1 - \frac{\zeta}{R_\alpha} + \left(\frac{\zeta}{R_\alpha}\right)^2\right); \quad \frac{1}{H_\beta} = \frac{1}{A_\beta}\left(1 - \frac{\zeta}{R_\beta} + \left(\frac{\zeta}{R_\beta}\right)^2\right) \tag{7}$$

Anisotropic 3D stress–strain relations are assumed for the constituent layers:

$$\sigma_{\mu\nu}^{(k)} = \overline{Q}_{\mu\nu\gamma\delta}^{(k)}\varepsilon_{\gamma\delta}^{(k)}; \quad \sigma_{\mu\zeta}^{(k)} = \overline{Q}_{\mu\zeta\nu\zeta}^{(k)}\varepsilon_{\nu\zeta}^{(k)} \tag{8}$$

($\mu,\upsilon,\gamma,\delta$ that in turn represent α,β; repeated indices imply the Einsteinian summation convention). Herein, the sandwich shells are treated as multilayered shells that are made of an arbitrary number of thin layers constituting the faces and of a thick intermediate layer constituting the honeycomb core, this assumption being successful in the studies [42,44,45] (core properties computed from the cellular properties; see, Gibson and Ashby [46]).

2.4. Displacement fields

The in-plane displacements are postulated to vary across the thickness as follows:

$$\begin{aligned} u_\alpha(\alpha,\beta,\zeta) = {} & \left(1 + \frac{\zeta}{R_\alpha}\right)u_\alpha^{(0)}(\alpha,\beta) - \zeta\frac{u_{\zeta,\alpha}^{(0)}(\alpha,\beta)}{A_\alpha} + \zeta(1 \\ & + (C_{2\alpha}(\alpha,\beta)\zeta + C_{3\alpha}(\alpha,\beta)\zeta^2))\gamma_\alpha^{(0)}(\alpha,\beta) + (O\zeta^4\ldots) \\ & + \sum_{k=1}^{S}\Phi_\alpha^{(k)}(\alpha,\beta)(\zeta - \zeta^{(k)})\mathscr{H}_{,k}(\zeta - \zeta^{(k)}) \end{aligned} \tag{9}$$

$$\begin{aligned} u_\beta(\alpha,\beta,\zeta) = {} & \left(1 + \frac{\zeta}{R_\beta}\right)u_\beta^{(0)}(\alpha,\beta) - \zeta\frac{u_{\zeta,\beta}^{(0)}(\alpha,\beta)}{A_\beta} + \zeta(1 \\ & + (C_{2\beta}(\alpha,\beta)\zeta + C_{3\beta}(\alpha,\beta)\zeta^2))\gamma_\beta^{(0)}(\alpha,\beta) + (O\zeta^4\ldots) \\ & + \sum_{k=1}^{S}\Phi_\beta^{(k)}(\alpha,\beta)(\zeta - \zeta^{(k)})\mathscr{H}_{,k}(\zeta - \zeta^{(k)}) \end{aligned} \tag{10}$$

The three displacements $u_\alpha^{(0)}, u_\beta^{(0)}, u_\zeta^{(0)}$ and the two shear rotations $\gamma_\alpha^{(0)}, \gamma_\beta^{(0)}$ of the points on the reference surface Ω are chosen as functional d.o.f., like in the classical models. The terms in the summations, which are characteristic of zig-zag models, represent contributions being continuous across the thickness, but with discontinuous derivatives at the layer interfaces. They enable an *a priori* fulfilment of the transverse shear stress contact conditions at the layer interfaces

$$\sigma_{\alpha\zeta}|_{(\zeta=^{(k)}\zeta^+)} = \sigma_{\alpha\zeta}|_{(\zeta=^{(k+1)}\zeta^-)} \tag{11}$$

$$\sigma_{\beta\zeta}|_{(\zeta=^{(k)}\zeta^+)} = \sigma_{\beta\zeta}|_{(\zeta=^{(k+1)}\zeta^-)} \tag{12}$$

suitably choosing the expressions of the continuity functions $\Phi_\alpha^{(k)}, \Phi_\beta^{(k)}$ as outlined in Section 3.1. $\mathscr{H}_{,k}$ is the Heaviside unit step function, i.e. $\mathscr{H}_{,k} = 1$ for $\zeta \geqslant \zeta^{(k)}$ and 0 for $\zeta < \zeta^{(k)}$. The coefficients $C_{2\alpha}$,$C_{3\alpha}$, $C_{2\beta}$,$C_{3\beta}$ are expressed in terms of the functional d.o.f. and their derivatives by enforcing the stress-free boundary conditions for the transverse shear stresses

$$\sigma_{\alpha\zeta}|^u = 0; \quad \sigma_{\alpha\zeta}|_l = 0; \quad \sigma_{\beta\zeta}|^u = 0; \quad \sigma_{\beta\zeta}|_l = 0 \tag{13}$$

at the upper $|^u$ and lower $|^l$ free surfaces. Non classical feature, the transverse displacement is approximated by the following higher-order representation:

$$\begin{aligned} u_\zeta(\alpha,\beta,\zeta) = {} & a(\alpha,\beta) + \zeta b(\alpha,\beta) + \zeta^2 c(\alpha,\beta) + \zeta^3 d(\alpha,\beta) \\ & + \zeta^4 e(\alpha,\beta) + (O\zeta^5\ldots) + \sum_{k=1}^{S-1}\Psi_\zeta^{(k)}(\alpha,\beta)(\zeta \\ & - {}^{(k)}\zeta)\mathscr{H}_k + \sum_{k=1}^{S-1}\Omega_\zeta^{(k)}(\alpha,\beta)(\zeta - {}^{(k)}\zeta)^2\mathscr{H}_k \end{aligned} \tag{14}$$

Two zig-zag contributions are incorporated in order to fulfil the stress contact conditions on the transverse normal stress and gradient:

$$\sigma_{\zeta\zeta}|_{(\zeta=^{(k)}\zeta^+)} = \sigma_{\zeta\zeta}|_{(\zeta=^{(k+1)}\zeta^-)}; \quad \sigma_{\zeta\zeta,\zeta}|_{(\zeta=^{(k)}\zeta^+)} = \sigma_{\zeta\zeta,\zeta}|_{(\zeta=^{(k+1)}\zeta^-)} \tag{15}$$

as prescribed by the elasticity theory, since they derive from the local equilibrium equations. The expressions of the continuity functions $\Psi_\zeta^{(k)}, \Omega_\zeta^{(k)}$ are determined in a straightforward way by enforcing the contact conditions (15) as shown in Section 3.1. The symbol a in Eq. (14) plays as the transverse displacement on the reference mid-plane $u_\zeta^{(0)}$. The still unknown coefficients b to e are determined by enforcing the boundary conditions on the transverse normal stress and its gradient at the upper and lower bounding surfaces:

$$\sigma_{\zeta\zeta}|^u = p^0|^u; \quad \sigma_{\zeta\zeta}|_l = p^0|_l; \quad \sigma_{\zeta\zeta,\zeta}|_l = \sigma_{\zeta\zeta,\zeta}|^u = 0 \tag{16}$$

(p^0 represents the transverse distributed loading). The displacement fields featured by Eqs. (9), (10) and (14) fulfil the following kinematic contact conditions that yield for perfect bonding:

$$\begin{aligned} u_\alpha|_{(\zeta=^{(k)}\zeta^+)} = u_\alpha|_{(\zeta=^{(k+1)}\zeta^-)}; \quad u_\beta|_{(\zeta=^{(k)}\zeta^+)} = u_\beta|_{(\zeta=^{(k+1)}\zeta^-)}; \quad u_\zeta|_{(\zeta=^{(k)}\zeta^+)} \\ = u_\zeta|_{(\zeta=^{(k+1)}\zeta^-)} \end{aligned} \tag{17}$$

The classical (CLST) and the first order shear deformation (FSDST) shell models can be particularised from Eqs. (9), (10) and (14) assuming a constant transverse displacement and the shear rotations as vanishing or being linear. The RHSDST model of Ref. [15], here referred as RHSDST0, RHSDST1, RHSDST2 for constant, linear or quadratic $1/H_\alpha$, $1/H_\beta$, is particularised assuming a constant transverse displacement and cubic the in-plane displacements. Of course, the corresponding plate models can be obtained disregarding the terms involving the radii of curvature.

The higher-order terms $(O\zeta^4\ldots)$ and $(O\zeta^5\ldots)$, that represent the adaptive part of the representation, give contributions of the following form:

$$P_J^n(\mathscr{H}_{n-1} - \mathscr{H}_n) + P_J^m(\mathscr{H}_{m-1} - \mathscr{H}_m) + \cdots \tag{18}$$

where P_J^n and P_J^m represent the hierarchic parts incorporated in the layer n and m, respectively (J stands for α, β). The Heaviside unit step functions $\mathscr{H}_{n-1}$ and $\mathscr{H}_{m-1}$ make the contributions P_J^n and P_J^m active at the interfaces $n-1$ and $m-1$, respectively, while $\mathscr{H}_{n-1} - \mathscr{H}_n$ and $\mathscr{H}_{m-1} - \mathscr{H}_m$ disable them at the interfaces n and m. Their explicit expressions are:

$$P_\alpha^v = A^\alpha \zeta^4 + B^\alpha \zeta^5 + C^\alpha \zeta^6 + D^\alpha \zeta^7 + E^\alpha \zeta^8 + \cdots \tag{19}$$

$$P_\beta^v = A^\beta \zeta^4 + B^\beta \zeta^5 + C^\beta \zeta^6 + D^\beta \zeta^7 + E^\beta \zeta^8 + \cdots \tag{20}$$

$$P_\zeta^v = A^\zeta \zeta^5 + B^\zeta \zeta^6 + C^\zeta \zeta^7 + D^\zeta \zeta^8 + E^\zeta \zeta^9 + \cdots \tag{21}$$

the symbol v being used for representing n and m. The contributions P_α^v, P_β^v and P_ζ^v hold for u_α, u_β and u_ζ, respectively. As a particular case, P_J^n can coincide with P_J^m, so the representation can be the same for a group of layers. The coefficients $A^\alpha \dots E^\alpha$, $A^\beta \dots E^\beta$, $A^\zeta \dots E^\zeta$, that are referred as the coefficients of the higher-order powers, are determined by enforcing local equilibrium conditions at selected points across the thickness or over a region, as outlined in Section 3.2.

3. Continuity functions and coefficients of higher-order powers

3.1. Continuity functions

The expressions of the continuity functions $\Phi_\alpha^{(k)}, \Phi_\beta^{(k)}, \Psi_\zeta^{(k)}, \Omega_\zeta^{(k)}$ are determined as outlined hereafter. In order to obtain expression that hold for general displacements U_α, U_β, U_ζ with any expansion order, the displacements are written in the following compact form

$$u_\alpha(\alpha,\beta,\zeta) = U_\alpha(\alpha,\beta,\zeta) + \sum_{k=1}^{S} \Phi_\alpha^{(k)}(\alpha,\beta)(\zeta-\zeta^{(k)})\mathscr{H}_k(\zeta-\zeta^{(k)}) \tag{22}$$

$$u_\beta(\alpha,\beta,\zeta) = U_\beta(\alpha,\beta,\zeta) + \sum_{k=1}^{S} \Phi_\beta^{(k)}(\alpha,\beta)(\zeta-\zeta^{(k)})\mathscr{H}_k(\zeta-\zeta^{(k)}) \tag{23}$$

$$u_\zeta(\alpha,\beta,\zeta) = U_\zeta(\alpha,\beta,\zeta) + \sum_{k=1}^{S-1} \Psi_\zeta^{(k)}(\alpha,\beta)(\zeta - {}^{(k)}\zeta)\mathscr{H}_k + \sum_{k=1}^{S-1} \Omega_\zeta^{(k)}(\alpha,\beta)(\zeta - {}^{(k)}\zeta)^2\mathscr{H}_k \tag{24}$$

According with this representation, the continuity functions are expressed as [42]:

$$\begin{aligned}\Phi_\alpha^{(k)} = {} & \mathbf{\Phi}_{u1}^{(k)}U_{\alpha,\alpha} + \mathbf{\Phi}_{u2}^{(k)}U_{\alpha,\beta} + \mathbf{\Phi}_{u3}^{(k)}U_{\alpha,\zeta} + \mathbf{\Phi}_{u4}^{(k)}U_{\beta,\alpha} + \mathbf{\Phi}_{u5}^{(k)}U_{\beta,\beta} \\ & + \mathbf{\Phi}_{u6}^{(k)}U_{\beta,\zeta} + \mathbf{\Phi}_{u7}^{(k)}U_{\zeta,\alpha} + \mathbf{\Phi}_{u8}^{(k)}U_{\zeta,\beta} + \mathbf{\Phi}_{u9}^{(k)}U_{\zeta,\zeta}\end{aligned} \tag{25}$$

$$\begin{aligned}\Phi_\beta^{(k)} = {} & \mathbf{\Phi}_{v1}^{(k)}U_{\alpha,\alpha} + \mathbf{\Phi}_{v2}^{(k)}U_{\alpha,\beta} + \mathbf{\Phi}_{v3}^{(k)}U_{\alpha,\zeta} + \mathbf{\Phi}_{v4}^{(k)}U_{\beta,\alpha} + \mathbf{\Phi}_{u5}^{(k)}U_{\beta,\beta} \\ & + \mathbf{\Phi}_{v6}^{(k)}U_{\beta,\zeta} + \mathbf{\Phi}_{v7}^{(k)}U_{\zeta,\alpha} + \mathbf{\Phi}_{v8}^{(k)}U_{\zeta,\beta} + \mathbf{\Phi}_{v9}^{(k)}U_{\zeta,\zeta}\end{aligned} \tag{26}$$

$$\begin{aligned}\Psi_\zeta^{(k)} = {} & \mathbf{\Psi}_1^{(k)}U_{\alpha,\alpha} + \mathbf{\Psi}_2^{(k)}U_{\alpha,\beta} + \mathbf{\Psi}_3^{(k)}U_{\alpha,\zeta} + \mathbf{\Psi}_4^{(k)}U_{\beta,\alpha} + \mathbf{\Psi}_5^{(k)}U_{\beta,\beta} \\ & + \mathbf{\Psi}_6^{(k)}U_{\beta,\zeta} + \mathbf{\Psi}_7^{(k)}U_{\zeta,\alpha} + \mathbf{\Psi}_8^{(k)}U_{\zeta,\beta} + \mathbf{\Psi}_9^{(k)}U_{\zeta,\zeta}\end{aligned} \tag{27}$$

$$\begin{aligned}\Omega_\zeta^{(k)} = {} & \mathbf{\Omega}_1^{(k)}U_{\alpha,\alpha\alpha} + \mathbf{\Omega}_2^{(k)}U_{\alpha,\alpha\beta} + \mathbf{\Omega}_3^{(k)}U_{\alpha,\alpha\zeta} + \mathbf{\Omega}_4^{(k)}U_{\alpha,\beta\beta} + \mathbf{\Omega}_5^{(k)}U_{\alpha,\beta\zeta} \\ & + \mathbf{\Omega}_6^{(k)}U_{\alpha,\zeta\zeta} + \mathbf{\Omega}_7^{(k)}U_{\beta,\alpha\alpha} + \mathbf{\Omega}_8^{(k)}U_{\beta,\alpha\beta} + \mathbf{\Omega}_9^{(k)}U_{\beta,\alpha\zeta} \\ & + \mathbf{\Omega}_{10}^{(k)}U_{\beta,\beta\beta} + \mathbf{\Omega}_{11}^{(k)}U_{\beta,\beta\zeta} + \mathbf{\Omega}_{12}^{(k)}U_{\beta,\zeta\zeta} + \mathbf{\Omega}_{13}^{(k)}U_{\zeta,\alpha\alpha} \\ & + \mathbf{\Omega}_{14}^{(k)}U_{\zeta,\alpha\beta} + \mathbf{\Omega}_{15}^{(k)}U_{\zeta,\alpha\zeta} + \mathbf{\Omega}_{16}^{(k)}U_{\zeta,\beta\beta} + \mathbf{\Omega}_{17}^{(k)}U_{\zeta,\beta\zeta} + \mathbf{\Omega}_{18}^{(k)}U_{\zeta,\zeta\zeta}\end{aligned} \tag{28}$$

since enforcing the interlaminar stress contact conditions a system of four relations is obtained at each interface that involves the continuity functions, the material properties of the adjacent layers, the generalised displacements u^j, v^j, w^j and their first and second order derivatives. Therefore, 45 continuity constants $\mathbf{\Phi}_{u1}^{(k)}, \dots, \mathbf{\Phi}_{u9}^{(k)}, \mathbf{\Phi}_{v1}^{(k)}, \dots, \mathbf{\Phi}_{v9}^{(k)}, \mathbf{\Psi}_1^{(k)}, \dots, \mathbf{\Psi}_9^{(k)}, \mathbf{\Omega}_1^{(k)}, \dots, \mathbf{\Omega}_{18}^{(k)}$ have to be determined at each interface. Owing to their arbitrary nature, the homologous displacements and displacement derivatives can be collected apart, giving rise to an appropriate system of 45 equations in the 45 unknown continuity constants.

Initially the second order derivatives of the generalized displacements are disregarded, except for certain terms that provide the necessary rank to the system of contact conditions in decomposed form. Their omission transforms ()(25)–(28) into a system of 27 equations in the 27 unknowns $\mathbf{\Phi}_{u1}^{(k)}, \dots, \mathbf{\Phi}_{u9}^{(k)}, \mathbf{\Phi}_{v1}^{(k)}, \dots, \mathbf{\Phi}_{v9}^{(k)}, \mathbf{\Psi}_1^{(k)}, \dots, \mathbf{\Psi}_9^{(k)}$, since the contributions by $\mathbf{\Omega}_1^{(k)}, \dots, \mathbf{\Omega}_{18}^{(k)}$ are disregarded. This system provides an approximate solution for the continuity functions $\mathbf{\Phi}_{u1}^{(k)}$ to $\mathbf{\Psi}_9^{(k)}$ that is used for determining approximate expressions for $\mathbf{\Omega}_1^{(k)}$ to $\mathbf{\Omega}_{18}^{(k)}$. The errors consequent to this approximation are recovered by introducing new continuity functions that are computed in a straightforward way by enforcing the stress contact conditions

$$\sigma_{xz}^J = \hat{\sigma}_{xz}^J + \sum_{k=1}^{S} \Lambda^{(k)}\mathscr{H}^{(k)} \tag{29}$$

$$\sigma_{yz}^J = \hat{\sigma}_{yz}^J + \sum_{k=1}^{S} \Theta^{(k)}\mathscr{H}^{(k)} \tag{30}$$

$$\sigma_{zz}^J = \hat{\sigma}_{zz}^J + \sum_{k=1}^{S} \Gamma^{(k)}\mathscr{H}^{(k)} \tag{31}$$

$$\sigma_{zz,z}^J = \hat{\sigma}_{zz,z}^J + \sum_{k=1}^{S} \Pi^{(k)}\mathscr{H}^{(k)} \tag{32}$$

at the interfaces. The derivatives of the d.o.f. involved by the present model are converted into their primitive functions in a way that preserves their contribution to the strain energy, as outlined hereafter, since could make it computationally inefficient. The scalar products of the displacement derivatives that appear in the expression of the strain energy $\|U_{\alpha,\alpha}\|, \|U_{\alpha,\beta}\|, \dots, \|U_{\beta,\alpha}\|, \|U_{\beta,\beta}\|, \dots$ are converted into the scalar products of their primitive functions $\|U_\alpha\|$, $\|U_\beta\|, \dots$ by equating their energy norms:

$$\|U_{\alpha,\alpha}\| = A\|U_\alpha\|; \quad \|U_{\alpha,\beta}\| = B\|U_\alpha\|; \quad \|U_{\beta,\alpha}\| = C\|U_\beta\| \tag{33}$$

The constants A, B, $C\dots$ are computed by expressing the unknown generalized displacements as a combination of trial functions $\left(u_{1,\dots}^1 u_{n,\dots}^1\right)$ with unknown amplitudes $\left(a_{1,\dots}^1 a_{n,\dots}^1\right)$, i.e. $U_\alpha = a_1^1 u_{1+\dots}^1 a_n^1 u_n^1$, $U_\beta = a_1^2 u_{1+\dots}^2 a_n^2 u_n^2$. The conversion of the derivatives of the displacements that appear in the strain energy turns into the conversion of the derivatives of the trial functions:

$$\left\langle u_{m,\alpha}^J u_{n,\alpha}^J \right\rangle = A\langle u_m^J u_n^J\rangle; \quad \left\langle u_{m,\beta}^J u_{n,\beta}^J \right\rangle = B\langle u_m^J u_n^J\rangle \tag{34}$$

(the symbol $\langle\rangle$ represents the integration across the thickness). The second order derivatives are converted in a similar way by:

$$\|U_{\alpha,\alpha}\| = {}^2A\|U_\alpha\|; \quad \|U_{\alpha,\alpha\beta}\| = {}^2B\|U_\alpha\|; \quad \|U_{\beta,\alpha\beta}\| = {}^2C\|U_\beta\| \tag{35}$$

computing the appropriate coefficients ${}^2A$, ${}^2B$, ${}^2C\dots$

3.2. Coefficients of higher-order powers

The displacements are now represented in the following form

$$u_\alpha = {}^\wedge U_\alpha + A^\alpha\zeta^4 + B^\alpha\zeta^5 + C^\alpha\zeta^6 + D^\alpha\zeta^7 + E^\alpha\zeta^8 + \cdots + \sum_{k=1}^{S} \Phi_\alpha^{(k)}\dots \tag{36}$$

$$u_\beta = {}^\wedge U_\beta + A^\beta\zeta^4 + B^\beta\zeta^5 + C^\beta\zeta^6 + D^\beta\zeta^7 + E^\beta\zeta^8 + \cdots + \sum_{k=1}^{S} \Phi_\beta^{(k)}\dots \tag{37}$$

$$u_\zeta = {}^\wedge U_\zeta + A^\zeta\zeta^4 + B^\zeta\zeta^5 + C^\zeta\zeta^6 + D^\zeta\zeta^7 + E^\zeta\zeta^8 + \cdots + \sum_{k=1}^{S} \Psi_\zeta^{(k)}\dots \tag{38}$$

that focuses on the higher-order terms of the polynomial representation. The coefficients $(A^{\alpha},\ldots,E^{\alpha},\ldots)$, $(A^{\beta},\ldots,E^{\beta},\ldots)$, $(A^{\zeta},\ldots,E^{\zeta},\ldots)$ of the higher-order powers of ζ are determined in closed form, by enforcing equilibria. In order to illustrate the procedure, the following stress derivatives appearing in the equilibria in local differential form are reported as examples:

$$\sigma_{\alpha,\alpha} = \left[{}^{(k)}C^{J}_{11}/H_{\alpha}\hat{}U_{\alpha} + A^{\alpha}\zeta^{4} + B^{\alpha}\zeta^{5} + C^{\alpha}\zeta^{6} + D^{\alpha}\zeta^{7} + E^{\alpha}\zeta^{8} + \cdots + \sum_{k=1}^{S}\Phi^{(k)}_{\alpha}\ldots\right)_{,\alpha}\Bigg]_{,\alpha} + \cdots + {}^{(k)}C^{J}_{16}\varepsilon_{\alpha\beta,\alpha} \tag{39}$$

$$\sigma_{\alpha\beta,\beta} = {}^{(k)}C^{J}_{61}\varepsilon_{\alpha\alpha,\beta} + \cdots + \left[{}^{(k)}C^{J}_{66}H_{\alpha}/H_{\beta}\left(\hat{}U_{\alpha} + A^{\alpha}\zeta^{4} + B^{\alpha}\zeta^{5} + C^{\alpha}\zeta^{6} + D^{\alpha}\zeta^{7} + E^{\alpha}\zeta^{8} + \cdots + \sum_{k=1}^{S}\Phi^{(k)}_{\alpha}\ldots/H_{\alpha}\right)_{,\beta}\right]_{,\beta} + \left[{}^{(k)}C^{J}_{66}H_{\beta}/H_{\alpha}\left(\wedge U_{\beta} + A^{\beta}\zeta^{4} + B^{\beta}\zeta^{5} + C^{\beta}\zeta^{6} + D^{\beta}\zeta^{7} + E^{\beta}\zeta^{8} + \cdots + \sum_{k=1}^{S}\Phi^{(k)}_{\beta}\ldots/H_{\beta}\right)_{,\alpha}\right]_{,\beta} \tag{40}$$

$$\sigma_{\alpha\zeta,\zeta} = \cdots + {}^{(k)}C^{J}_{54}\varepsilon_{\beta\zeta,\zeta} + \left[{}^{(k)}C^{J}_{55}H_{\alpha}\left[\hat{}U_{\alpha} + A^{\alpha}\zeta^{4} + B^{\alpha}\zeta^{5} + C^{\alpha}\zeta^{6} + D^{\alpha}\zeta^{7} + E^{\alpha}\zeta^{8} + \cdots + \sum_{k=1}^{S}\Phi^{(k)}_{\alpha}\ldots/H_{\alpha}\right)_{,\zeta} + {}^{(k)}C^{J}_{55}/H_{\alpha}\left[\hat{}U_{\zeta} + A^{\zeta}\zeta^{4} + B^{\zeta}\zeta^{5} + C^{\zeta}\zeta^{6} + D^{\zeta}\zeta^{7} + E^{\zeta}\zeta^{8} + \cdots + \sum_{k=1}^{S}\Psi^{(k)}_{\zeta}\ldots\right)_{,\alpha}\right]_{,\zeta} \tag{41}$$

A system of independent equations is obtained that allows to determine all the unknown parameters, since any number of points at which enforce equilibria can be chosen. The expressions of the derivatives of A^{α}, A^{β}, A^{ζ} are determined disregarding the derivatives of the higher-order terms B^{α}, B^{β}, $B^{\zeta},\ldots,E^{\zeta}$. In a similar way, the derivatives of B^{α}, B^{β}, B^{ζ} are determined disregarding C^{α}, C^{β}, C^{ζ}, and so on, since in this way the higher order models contain the lower-order ones as particular cases.

These expressions are substituted into the governing equations; where necessary, integrations (indefinite integrals) are carried out by substituting the d.o.f expressed in terms of the trial functions. The derivation of the governing equations is omitted since the standard techniques can be used.

The stress continuity conditions can be easily restored at the points where the representation is varied, since the enforcement of any condition of interest implies the addition of a new power term to the expansions (36)–(38), which is computed by the condition itself.

Owing to the variable representation used, a consistent behaviour can be obtained with a suited choice of the coefficients of higher-order powers. For instance, zero normal and transverse shear stresses in presence of nonzero bending strains could be enforced in order to prevent Poisson's locking when approaching the thick limit, as well as a state of zero transverse shear stress in presence of nonzero bending strain, in order to avoid shear locking when approaching the thin limit. Another important condition that can be enforced is a non vanishing transverse shear at clamped edges, although the displacements and their derivatives vanish, to avoid the poor behaviour of the models with displacements and shear rotations as functional d.o.f.

4. Numerical applications

Just simply-supported cross-ply cylindrical shells in cylindrical bending under sinusoidal loading are considered. In fact for this case the exact three-dimensional elasticity solution can be determined, as shown by Ren [7]. Furthermore this option offers the possibility of comparing the results with many others in literature, since it is customary chosen by the researchers (see, e.g. [21,22,32,41]). To enable the comparison with other models, the angle ψ substented by the ends is assumed equal to $\pi/3$, in such a way β traces a circumferential path of length $R_{\beta}\psi$. In the other direction $R_{\alpha} = \infty$ is assumed. The distributed loading is represented as $p^{0}|^{u} = P \sin(\pi\beta/\psi)$. Most of the results refer to a thickness ratio $S = R/h$ $(R = R_{\beta})$ of 4 because, although unrealistic for engineering applications, it constitutes a severe test for the models; for this reason it is customary chosen by the researchers. According with Ref. [7], displacements and stresses are reported at $\beta = \psi/2$ or at $\beta = 0$ where they assume their maximum, in the following normalised form:

$$\bar{u}_{\beta}(\zeta) = \frac{u_{\beta}(\zeta,0)}{q^{0}h}; \quad \bar{u}_{\zeta}(\zeta) = \frac{u_{\zeta}(\zeta,\psi/2)}{q^{0}h};$$
$$\bar{\sigma}_{\beta\beta}(\zeta) = \frac{\sigma_{\beta\beta}(\zeta,\psi/2)}{q^{0}S^{2}}; \quad \bar{\sigma}_{\beta\zeta}(\zeta) = \frac{\sigma_{\beta\zeta}(\zeta,0)}{q^{0}S^{2}h};$$
$$\bar{\sigma}_{\zeta\zeta}(\zeta) = \frac{\sigma_{\zeta\zeta}(\zeta,\psi/2)}{q^{0}} \tag{42}$$

The variation of the d.o.f. over the reference plane is assumed as a trigonometric series expansion, within the framework of the Galerkin's method:

$$u^{(0)}_{\beta} = \sum_{i=1}^{Q1} A^{u\beta}\cos(i\pi\beta/\psi); \quad u^{(0)}_{\zeta} = \sum_{i=1}^{Q2} A^{u\zeta}\sin(i\pi\beta/\psi);$$
$$\gamma^{(0)}_{\beta} = \sum_{i=1}^{Q3} A^{\gamma\beta}\cos(i\pi\beta/\psi) \tag{43}$$

Only the first term is retained with the RHSDST model, as it gives the exact solution to governing equations. On the contrary, several terms (up to 6) should be retained with the present model.

Numerical applications are presented for laminated shells, with the purpose of assessing whether the present model can accurately predict the interlaminar stresses without post-processing. Results for sandwich shells with damaged faces or a damaged core are also presented since, owing to their abruptly changing material properties across the thickness, represent very severe tests cases.

4.1. Laminated shells

The same cases already examined in Refs. [7,21,22,32,41] are considered, in order to asses the improvements brought by the present adaptive representation of displacements. According, the following material properties are chosen: $E_L/E_T = 25$; $G_{LT}/E_T = 0.5$; $G_{TT}/E_T = 0.2$; $\upsilon_{LT} = 0.25$. Table 1 presents the normalised deflection $\bar{}u_{\zeta}$ at $\zeta = 0$ of 0°/90° unsymmetric and 90°/0°/90° symmetric cross-ply shells in cylindrical bending under sinusoidal loading. The thickness ratios $S = R/h$ $(R = R_{\beta})$ considered range from 4 up to 500. Here 0° means fibres parallel to the β direction, while 90° fibres perpendicular to β. The symbol BM represents the basic model, i.e. the RHSDST model of Ref. [22]. The symbols 0, 1, 2 rep-resent the expansion order of the reciprocals of the Lamé coeffi-cients $1/H_{\alpha}$, $1/H_{\beta}$ (see, Eq. (7)) used with the basic model. All the

Table 1
Normalised deflection of simply supported cross-ply shells in cylindrical bending under sinusoidal loading, for different thickness ratios.

$S = R/h$	Dennis–Palazotto [8]	BM 0 [15]	BM 1 [15]	BM 2 [15]	Present[a]	Exact (Ren [4])
0°/90°						
4	0.6993	0.6398	0.6589	0.6554	0.8316	0.854
10	0.4593	0.4408	0.4472	0.4462	0.4814	0.493
50	0.4048	0.3939	0.3958	0.3957	0.4048	0.409
100	0.4018	0.3911	0.3920	0.3920	0.4014	0.403
500	0.3998	0.3893	0.3895	0.3895	0.3991	0.399
90°/0°/90°						
4	0.382	0.3771	0.4817	0.4709	0.4506	0.457
10	0.128	0.1343	0.1386	0.1381	0.1468	0.144
50	0.0796	0.0796	0.0797	0.0797	0.0800	0.0808
100	0.0781	0.0778	0.0778	0.0778	0.0781	0.0787
500	0.0774	0.0773	0.0773	0.0773	0.0775	0.0773

[a] The expansion order across the thickness is 6 for u_α and 4 for u_ζ. A quadratic representation of the reciprocals of Lamè coefficients is used.

results by the present model appearing in Table 1 refer to a second order expansion of these coefficients and a sixth order expansion of the in-plane displacements U_α, U_β and a fourth expansion for the transverse displacement. U_ζ in Eqs. (22)–(24). The distributions across the thickness of the in-plane and transverse shear stresses $\bar{\sigma}_{\beta\beta}$, $\bar{\sigma}_{\beta\zeta}$ are shown in Fig. 1a–f, with the purpose of focusing the different behaviour of the present model and of the basic model. Fig. 1a represents the through-the-thickness variation of the in-plane stress $\bar{\sigma}_{\beta\beta}$ for a 0°/90° lay-up and S = 4, while Fig. 1b represents the transverse shear stress $\bar{\sigma}_{\beta\zeta}$. Fig. 1c and d report the in-plane stress $\bar{\sigma}_{\beta\beta}$ and the transverse shear stress $\bar{\sigma}_{\beta\zeta}$ for a 90°/0°/90° shell with S = 4, respectively. Fig. 1e shows the transverse shear stress $\bar{\sigma}_{\beta\zeta}$ for the same lay-up and S = 10, while Fig. 1f shows the same stress for a 90°/0°/90°/0°/90° five layer cross-ply shell with S = 5 and S = 10. The through-the-thickness variation of the transverse displacement $\bar{u}_\zeta$ is omitted in order to contain the length of the paper, being very small and similar to that of undamaged sandwich shells. The variation of the in-plane displacement $\bar{u}_\beta$ and of $\bar{\sigma}_{\zeta\zeta}$ are also omitted for the same reason. These distributions will be considered in the case of sandwich shells, being different with or without damage.

It appears by the numerical results that the present model predicts the displacement and stress fields with an improved accuracy with respect to the basic shell model of Ref. [22], either for thin or thick shells. While the basic model can quite accurately capture $\bar{\sigma}_{\beta\beta}$ from the constitutive equations and consequently capture $\bar{\sigma}_{\beta\zeta}$ by integrating the local differential equilibrium equations, the present model always provides accurate stress predictions by the constitu-tive equations. Although improved predictions of the in-plane stress $\bar{\sigma}_{\beta\beta}$ are also obtained, this represents the most important advantage of the present five d.o.f. model. Indeed, this property makes it suited for damage analysis, and in particular for impact studies, owing to the a low memory occupation. As it appears from Table 1, the pres-ent model can also more accurately predict the deflections with re-spect to the basic model, owing to its improved representation of the transverse displacement. Obviously, the higher-order terms play a marginal role in the case of very thin shells.

The improved predictive capability of the present model results in computational costs saving, since the overall processing time of the present model is lower than that of the basic shell model that requires a quite long post-processing for obtaining a comparable accuracy. If the processing time on a laptop computer of the FORTRAN computational model for$S$ = 4 is normalised to the case of the basic model, it appears that the post-processing operations take about the 60% of the overall processing time, while the present model, without any post-processing, requires an overall computational time that is 70% of the one of the basic model.

This advantage becomes consistent when repeated computations are required, since the continuity constants and of the coefficients of higher-order terms, whose computation takes up to 15% of the overall time, need to be determined once for all for any lamination sequence, loading and boundary conditions.

4.2. Sandwich shells

Cylindrical sandwich shells with S = 4 and 10, in cylindrical bending under the same loading and boundary conditions than in the previous section, and with the material properties and lay-up of Ref.[29] are considered. The face layers are made of materials 1 to 3, while the core is made of material 4, whose mechanical properties are as follows. MAT 1: $E_1 = E_3 = 1$, $G_{13} = 0.2$ (GPa), $\upsilon_{13} = 0.25$; MAT 2: $E_1 = 33, E_3 = 1$, $G_{13} = 8$, $\upsilon_{13} = 0.25$; MAT 3: $E_1 = 25, E_3 = 1$, $G_{13} = 0.5, \upsilon_{13} = 0.25$; MAT 4: $E_1 = E_3 = 0.05$, $G_{13} = 0.0217$, $\upsilon_{13} = 0.15$. MAT 1 is rather weaker in tension–compression and shear compared to MAT 2, whereas MAT 3 is stiff in tension–compression but rather weak in shear. As usual, MAT 4 compared to the other materials is very weak in tension–compression and rather weak in shear. The sandwich shell is simulated as a multilayered shell with a (MAT 1/ 2/3/1/3/4)$_s$ stacking sequence and the following thickness ratios of the constituent layers (0.010/0.025/0.015/0.020/0.030/0.4)$_s$. A s shown in Ref. [29], this combination of materials and the lay-up chosen result in rather intricate displacement and stress distributions across the thickness that are more difficult to capture of those of laminates. A very refined subdivision into computational layers was required by the SZZ model of Ref. [29] for obtaining accurate stress predictions from the constitutive equations, in particular when damage was considered. The integration of the local differen-tial equilibrium equations reduced the overall computational effort, although the post-processing was rather laborious.

The purpose now is to assess whether the displacement and stress distributions can be still captured by the present shell model without post-processing, as occurred in the previous case of laminated shells. The exact three dimensional solution for the actual case has been computed by the authors with the technique of Ren [7], since at their best knowledge results were not available in the literature for the constituent materials here considered and in presence of damage. To this purpose the damage is unreal-istically assumed as spreading over the entire length in the β direc-tion, it being just considered for having abruptly changing material properties across the thickness. A more realistic, localized distribution will be easily simulated once finite elements based on the present model will be developed. In the current case the damage is simulated with a degradation of the elastic properties, according to the ply-discount theory. A factor 10^{-2} is used for simulating the residual properties in presence of damage. A damaged upper face is

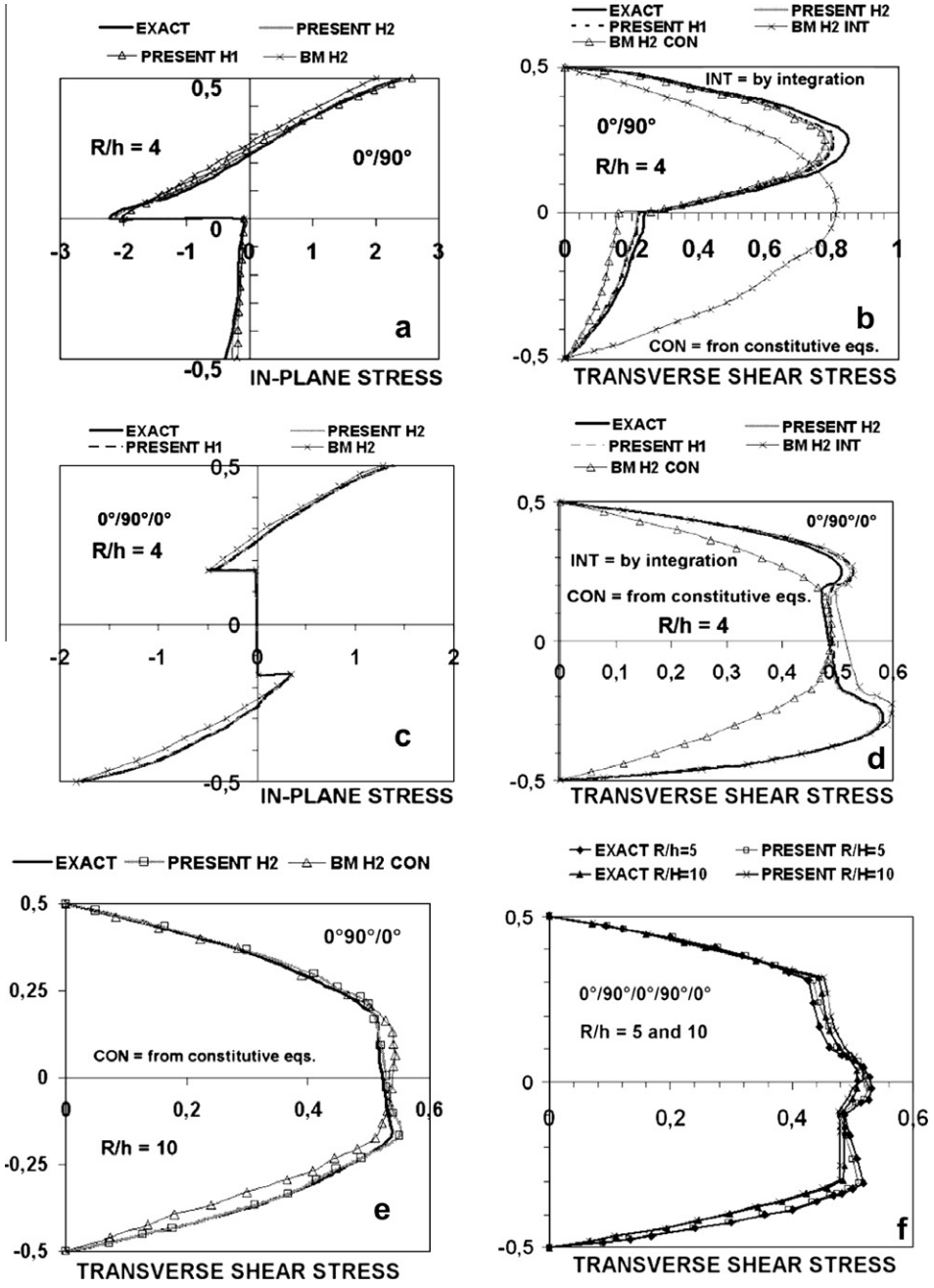

Fig. 1. Displacement and stress fields across the thickness of simply-supported, laminated shells undergoing sinusoidal transverse distributed loading (the vertical coordinate is ζ/h).

simulated reducing E_3 with this factor, whereas a damaged core is simulated reducing G_{13} in the same way. This choice is made in order the modelling of u_ζ and $\sigma_{\zeta\zeta}$ is crucial in the former case, while $\sigma_{\beta\zeta}$ is crucial in the latter case.

Fig. 2a to d show the through-the thickness distribution of the in-plane and transverse displacements $\bar{u}_\beta$, $\bar{u}_\zeta$ and of the out-of-plane stresses $\bar{\sigma}_{\beta\zeta}$, $\bar{\sigma}_{\zeta\zeta}$ respectively, as predicted by the pres-ent model and by the exact elasticity solution for S = 4 and 10, when the sandwich is undamaged, the upper face is damaged, or the core is damaged. The solution by the present model is obtained assuming a sixth order expansion of the displacementsU_α, U_β, U_ζ in Eqs. ()(22)–(24). Note that an interesting capability of the present model is the possibility of re-computing higher-order coefficients at new points across the thickness without increasing the expansion order of the representation. Therefore coefficients that have been already determined can be updated for refining the solution without any increase of the polynomial degree. This allows to account for the local variations of the solution in a more accurate and computationally more efficient way.

Owing to position of the neutral plane close to the lower face when the upper face is damaged, a change of sign of the transverse displacement occurs for S = 4, as shown in Fig. 2b.

The numerical results of Fig. 2a–d, which have been obtained with a second order expansion of the reciprocals of theA Lamé coefficients, show the capability of the present model to predict the distributions of the stresses across the thickness without post-processing, as well the displacements, even with abruptly changing material properties across the thickness. The steepest gradients consequent to this variation, that are magnificated by the presence of damage, are predicted with a lower computational

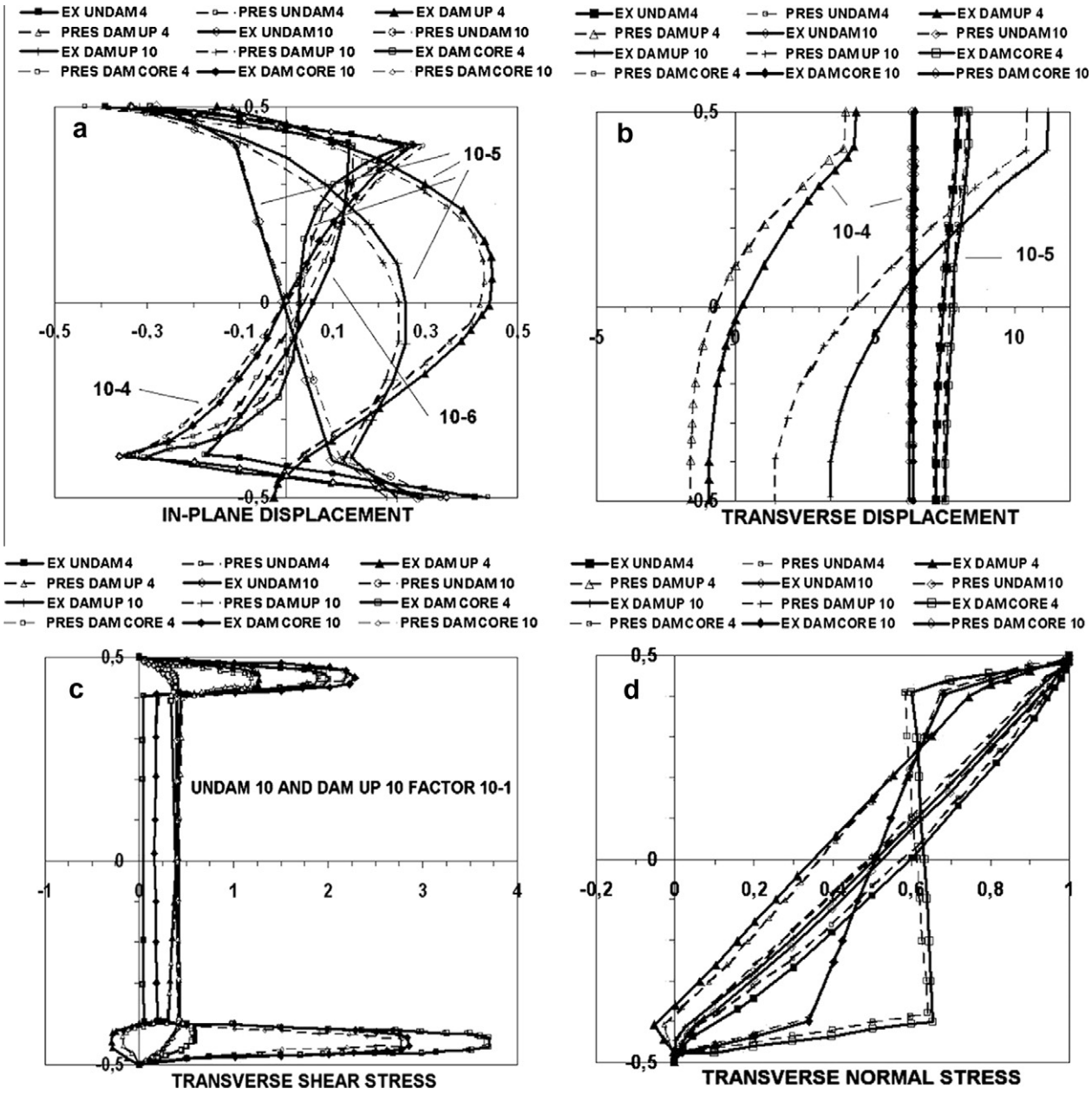

Fig. 2. Displacement and stress fields across the thickness of undamaged and damaged, simply-supported, sandwich shells undergoing sinusoidal transverse distributed loading: cases. Symbols: EX *aa* = exact; UNDAM *aa* = undamaged; DAM UP *aa* = damaged upper face; DAM CORE *aa* = damaged core (*aa* represents the thickness ratio $S = R/h$; the vertical coordinate is ζ/h).

effort by the present model, despite the additional computations involved for defining the coefficients of the higher-order powers.

The overall processing time required by the present model is lower than for the basic model, which requires to be post-processed for a comparable accuracy, in all the examined cases. It is also lower with respect to the sublaminate model of Ref. [29], which requires either the subdivision into many computational layers, consequently resulting in a larger memory occupation, or the use of post-processing operations. It appears that the processing time required by the post-processing phase is up to 65% the overall processing time for the basic model when the sandwich shell is undamaged, up to 68% when the upper face is damaged and 66% when the core is damaged. If the processing time is normalised to the case of the undamaged sandwich analysed by the basic model, it results that the present model, which does not need to be post-processed, requires an overall processing time that is just 75% in the undamaged case and 82% when the upper face is damaged and 79% when the core is damaged. In the undamaged case, the analysis by the model of Ref. [29] with subdivision into computational layers (up to 55 without post-processing) requires a processing time that is just 18% greater and a larger memory occupation than for the present model. The time increases to 20% and 19%, respectively, when the upper face or the core are damaged. If the model of Ref. [29] is post-processed, a single computational layer can be employed, but op to 45% of the overall time, which is larger by 15% with respect to the present model, is required for this operation.

5. Concluding remarks

A multilayered shell model with the classical five mid-plane functional d.o.f. for analysis of laminated and sandwich shell has

been developed; it can capture the through-the-thickness distribution of interlaminar stresses from constitutive equations. This capability is enabled by a variable zig-zag representation of the displacements whose higher-order coefficients are determined enforcing equilibrium conditions at discrete points across the thickness. The numerical results show that the present model can accurately capture the stress fields of thick laminated and sandwich shells with an expansion order of the displacements up to 6. Although it requires the computation of higher coefficients, its computational effort is lower than that of the counterpart lower order model with fixed representation, which requires to be post-processed for obtaining a comparable accuracy, as well as of a discrete-layer model with subdivision of the constituent layers into computational layers.

References

[1] Savoia M, Reddy JN. A variational approach to three-dimensional elasticity solutions of laminated composite plates. J Appl Mech 1992;59:166–75.
[2] Savoia M, Reddy JN. Three-dimensional thermal analysis of laminated composite plates. Int J Solids Struct 1995;32:593–608.
[3] Savoia M, Tralli A, Laudiero F. A refined theory for laminated beams: part II – an iterative variational approach. Meccanica 1993;28:217–25.
[4] Burton WS, Noor AK. Assessment of computational models for sandwich panels and shells. Comput Methods Appl Mech 1995;123:125–51.
[5] Reddy JN. Mechanics of laminated composite plates and shells: theory and analysis. 2nd ed. Boca Raton, FL: CRC Press; 2003.
[6] Reddy JN. A layerwise shell theory with applications to buckling and vibration of cross-ply laminated circular cylindrical shells. Research Report CCMS-92-01, Center for Composite Materials and Structures, Virginia Polytechnic Institute and State University, Blacksburg, VA, USA; 1992.
[7] Ren JG. Exact solutions for laminated cylindrical shells in cylindrical bending. Compos Sci Technol 1987;29:169–87.
[8] Wu CP, Tarn JQ, Chi SM. Three-dimensional analysis of doubly curved laminated shells. J Eng Mech 1996;122(5):391–401.
[9] Sheng HY, Ye JQ. A three-dimensional state space finite element solution for laminated composite cylindrical shells. Comput Methods Appl Eng 2003;192:2441–59.
[10] Wu CP, Liu CC. Mixed finite element analysis of thick doubly curved laminated shells. J Aerosp Eng 1995;8:43–53.
[11] Ascione L, Fraternali F. A penalty model for the analysis of composite curved beams. Comput Struct 1992;45:985–99.
[12] Fraternali F, Reddy JN. A penalty model for the analysis of laminated composite shells. Int J Solids Struct 1993;30(24):3337–55.
[13] Barbero EJ, Reddy JN. Modeling of delamination in composite laminates using a layer-wise plate theory. Int J Solids Struct 1991;28(3):373–88.
[14] Lee KH, Cao L. A predictior–corrector zig-zag model for the bending of laminated composite plates. Int J Solids Struct 1996;33(6):879–97.
[15] Dennis ST, Palazotto AN. Laminated shell in cylindrical bending, two-dimensional approach vs exact. AIAA J 1991;29:647–50.
[16] Jing HS, Tzeng KG. Refined shear deformation theory of laminated shells. AIAA J 1993;31:765–73.
[17] Di Sciuva. An improved shear deformation theory for moderately thick anisotropic shells and plates. J Appl Mech 1987;54:589–96.
[18] Di Sciuva, Icardi U. Discrete-layer models for multilayered anisotropic shells accounting for the interlayers continuity conditions. Meccanica 1993;28:281–91.
[19] Xavier PB, Lee KH, Chew CH. An improved zig-zag model for the bending of laminated composite shells. Compos Struct 1993;26:123–38.
[20] Cho M, Kim KO, Kim MH. Efficient higher-order shell theory for laminated composites. Compos Struct 1996;34:197–212.
[21] Icardi U. Cylindrical bending of laminated cylindrical shells using a modified zig-zag theory. Struct Eng Mech 1998;6(5):497–516.
[22] Icardi U, Ruotolo R. Laminated shell model with second-order expansion of the reciprocals of Lame coefficients Ha, Hb and interlayer continuities fulfilment. Compos Struct 2002;56:293–313.
[23] Oh J, Cho M. Higher order zig-zag theory for smart composite shells under mechanical-thermo-electric loading. Int J Solids Struct 2007;44(1):100–27.
[24] Averill RC, Yip YC. An efficient thick beam theory and finite element model with zig-zag sublaminates approximations. AIAA J 1996;34:1626–32.
[25] Cho YB, Averill RC. An improved theory and finite element model for laminated composite and sandwich beams using first-order zig-zag sublaminate approximations. Compos Struct 1997;37:281–98.
[26] Aitharaju VR, Averill RC. C° zig-zag kinematic displacement models for the analysis of laminated composites. Mech Compos Mater Struct 1999;6:31–56.
[27] Aitharaju VR, Averill RC. C° zig-zag finite element for analysis of laminated composites beams. J Eng Mech 1999;125:323–30.
[28] Yip YC, Averill RC. Three-dimensional laminated plate finite element with higher-order zig-zag sublaminate approximations. Int J Comput Eng Sci 2001;2:137–80.
[29] Icardi U. Layerwise mixed element with sublaminates approximation and 3D zig-zag field, for analysis of local effects in laminated and sandwich composites. Int J Numer Meth Eng 2007;70:94–125.
[30] Cho M, Kim KO, Kim MH. Efficient higher-order shell theory for laminated composites. Compos Struct 1996;34:197–212.
[31] Li XY, Liu D. Generalized laminate theories based on double superposition hypothesis. Int J Numer Meth Eng 1997;40:1197–212.
[32] Zhen W, Wanji C. A global–local higher order theory for multilayered shells and the analysis of laminated cylindrical shell panels. Compos Struct 2008;84:350–61.
[33] Reddy JN, Liu CF. A higher-order shear deformation theory of laminated elastic shells. Int J Eng 1985;23:319–30.
[34] Dennis ST, Palazotto AN. Laminated shell in cylindrical bending, two-dimensional approach vs exact. AIAA J 1991;29:647–50.
[35] Xavier PB, Lee KH, Chew CH. An improved zig-zag model for the bending of laminated composite shells. Compos Struct 1993;26:123–38.
[36] Jing HS, Tzeng KG. Refined shear deformation theory of laminated shells. AIAA J 1993;31:765–73.
[37] Reddy JN, Starnes Jr JH. General buckling of stiffened circular cylindrical shells according to a layerwise theory. Comput Struct 1993;49(4):605–16.
[38] Savoia M, Reddy JN. Post-buckling behavior of stiffened cross-ply cylindrical shells. J Appl Mech 1994;61:998–1000.
[39] Cho M, Kim KO, Kim MH. Efficient higher-order shell theory for laminated composites. Compos Struct 1996;34:197–212.
[40] Fraternali F, Bilotti G. Non-linear elastic stress analysis in curved composite beams. Comput Struct 1997;199(62):837–69.
[41] Vidal P, Polit O. A refined sine-based finite element with transverse normal deformation for the analysis of laminated beams under thermomechanical loads. J Mech Mater Struct 2009;4:1127–55.
[42] Icardi U, Ferrero L. Layerwise zig-zag model with selective refinement across the thickness. Int J Numer Meth Eng, in press. doi: 10.1002/nme.2933.
[43] Icardi U. Higher-order zig-zag model for analysis of thick composite beams with inclusion of transverse normal stress and sublaminates approximations. Composites: Part B 2001;32:343–54.
[44] Icardi U, Ferrero L. Optimisation of sandwich panels with functionally graded core and faces. Compos Sci Technol 2009;69:575–85.
[45] Icardi U, Ferrero L. Impact analysis of sandwich composites based on a refined plate element with strain energy updating. Compos Struct 2009;89:35–51.
[46] Gibson LJ, Ashby MF. Cellular solids: structure and properties. 2nd ed. Cambridge University Press; 1997. ISBN:0521 495601.